JOC Article
pubs.acs.org/joc

Highly Sensitive Water-Soluble Fluorescent pH Sensors Based on the 7-Amino-1-methylquinolinium Chromophore

Wolter F. Jager,*[,†] Tessel S. Hammink,[†] Otto van den Berg,[§] and Ferdinand C. Grozema[∥]

[†]*Laboratory of NanoOrganic Chemistry,* [§]*Laboratory of NanoStructured Materials, and* [∥]*Laboratory of Optoelectronic Materials, Department of Chemical Engineering DelftChemTech, Delft University of Technology, Julianalaan 136, 2628BL Delft, The Netherlands*

w.f.jager@tudelft.nl

Received November 13, 2009

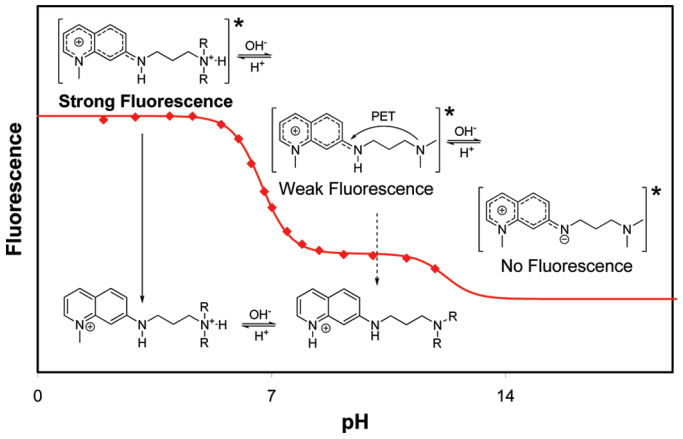

Highly sensitive water-soluble fluorescent pH sensors have been synthesized employing the 7-amino-1-methylquinolinium (7AMQ) chromophore. These compounds, which contained oligomethylene spacers and substituted amine receptor units, were prepared in high yields and purity by a single reaction from the readily available 7-fluoro-1-methylquinolinium iodide. Density functional theory (DFT) and semiempirical INDO/s calculations have been performed to describe the ground state and the locally excited state of the chromophore. The photophysics and the sensor characteristics have been investigated. Dissociation constants pK_A* ranging from 5.8 to 9.9 have been obtained. An additional quenching process at pH 11, due to excited state deprotonation at N7, has been observed. Fluorescence quantum yields in the protonated "on-state" between 0.75 and 0.85 and fluorescence enhancements (FE) between 2 and 55 were determined. These values are significantly higher than those of molecules based on other CT-chromophores that contain identical spacer−receptor units. The high fluorescence enhancements may be explained by the low rate of fluorescence ($\sim 6 \times 10^7\ s^{-1}$) and the high excited state reduction potential (~1.6 eV) of the 7AMQ chromophore.

Introduction

Molecular probes and sensors are the ultimate in device miniaturization.[1] Fluorescent molecules[2] take a special place due to detection limits down to the single molecule. Various studies report the detection of individual molecules, predominantly by Scanning Near-Field Optical Microscopy SNOM techniques.[3] For the detection of bio(macro)molecules labeled with appropriate fluorescent markers, detection limits in the subattamolar range ($< 10^{-18}$ mol) have been reported for routine measurements.[4]

(1) (a) *Molecular Switches*; Feringa, B. L., Ed.; Wiley-VCH: Weinheim, Germany, 2001. (b) Balzani, V.; Venturi, M.; Credi, A. *Molecular Devices and Machines*; Wiley-VCH: Weinheim, Germany, 2003.

(2) (a) Lakowicz, J. R. *Principles of Fluorescence Spectroscopy*; Kluwer Academic and Plenum Publishers: New York, 1999. (b) Valeur, B. *Molecular Fluorescence*; Wiley-VCH, Weinheim, Germany, 2001.

(3) Vallee, R. A. L.; Tomczak, N.; Kuipers, L.; Vancso, G. J.; van Hulst, N. F. *Phys. Rev. Lett.* **2003**, *91*, 038301.

(4) For examples, see: Haugland, R. P. In *Handbook of Fluorescent Probes and Research Chemicals*, 9th ed; Molecular Probes: Eugene, OR, 2002.

DOI: 10.1021/jo902225k Published on Web 03/02/2010

SCHEME 1. Synthesis of Compounds 2−4

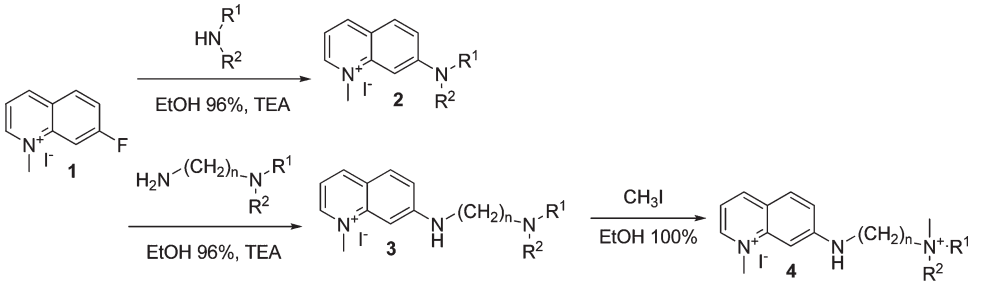

2a: R^1=H, R^2=CH_3
2b: R^1=H, R_2=C_2H_5
2c: R^1=H, R_2=C_4H_9
2d: R^1=R^2=CH_3

3a: n=2, R^1=R^2=H
3b: n=3, R^1=R^2=H
3c: n=4, R^1=R^2=H
3d: n=2, R^1=R^2=CH_3
3e: n=3, R^1=R^2=CH_3
3f: n=2, R^1,R^2=-$C_2H_4OC_2H_4$-
3g: n=3, R^1,R^2=-$C_2H_4OC_2H_4$-

4a: n=2, R^1=R^2=CH_3
4b: n=3, R^1=R^2=CH_3
4c: n=2, R^1,R^2=-$C_2H_4OC_2H_4$-
4d: n=3, R^1,R^2=-$C_2H_4OC_2H_4$-

Fluorescent molecular sensors[5] contain a receptor unit that is attached to a fluorescent chromophore in such a fashion that the binding of a specific analyte is translated into changes in emission. If the receptor unit is in (electronic) conjugation with the fluorophore, notably being part of a donor or acceptor unit in a push−pull system, binding of an analyte will induce significant shifts of the fluorescence wavelength. In such cases, generally referred to as chromophore−receptor sensors, ratiometric sensors are obtained,[6] providing that both the free sensor and the sensor−analyte complex are highly fluorescent. In the alternative chromophore−spacer−receptor approach, the receptor is not in conjugation with the chromophore, and the binding of an analyte will not change the color of the emission. Instead, the extent of fluorescence quenching by the receptor will be modulated, and "light-up" fluorescent sensors are obtained. The general quenching mechanism for these sensors is photoinduced electron transfer (PET),[7] an event that can occur through space and does not require electronic conjugation through a π-framework. The design of chromophore−spacer−receptor sensors is modular, which implies that all components can be altered independently, giving rise to predictible changes in sensor characteristics in most cases. Ionic species like protons,[8] metal ions,[9] anions,[10] or DNA strands[11] have been detected very efficiently, using sensors with appropriate receptor units. On the basis of a series of polymer bound sensors, a kit for fast blood analysis has been developed.[12] When CT chromophores are used in the chromophore−spacer−receptor design, fluorescence quenching is often accompanied by moderate shifts in absorption and emission spectra, and therefore their characteristics are generally in between those of ratiometric and light-up sensors.

Recently, we have reported the synthesis of 7-amino-1-methyl-quinolinium iodides (**2**) from 7-fluoro-1-methylquinolinium iodide (**1**) by a facile nucleophilic aromatic substitition at the 7-position, see Scheme 1.[13] Compound **1** is a very versatile synthon that is readily synthesized on a multigram scale. For **2** high fluorescence quantum yields in water and excellent thermal and photochemical stability have been reported. 1-Methyl-7-dimethylaminoquinolinium tetrafluoroborate, for example,[14] has been used as a color-shifting mobility sensitive fluorescent probe for polymer characterization at elevated temperatures. A number of 7-piperazino and 7-*N*-alkylamino derivatives have been synthesized and preliminary experiments have shown that these compounds are highly sensitive fluorescent pH sensors. It should be mentioned that quinoline and quinolinium derivatives have been employed as fluorescent sensors. Unsubstituted quinolinium ions have been used as in vivo Cl^- sensors.[15] The ability to detect Cl^- ions is based on the exceptionally high excited state reduction potential $E^*(S_1)_{red}$ of this cationic chromophore, which enables *inter*molecular PET. The 6-hydroxyquinoline motif has been recognized as a very versatile building block for the construction of cation sensors.[16] The cation sensing is based on the 3:1 complexation

(5) For reviews on fluorescent sensors, see: (a) de Silva, A. P.; Gunaratne, H. Q. N.; Gunnlaugsson, T.; Huxley, A. J. M.; McCoy, C. P.; Rademacher, J. T.; Rice, T. E. *Chem. Rev.* **1997**, *97*, 1515–1566. (b) Callan, J. F.; de Silva, A. P.; Magri, D. C. *Tetrahedron* **2005**, *61*, 8551–8588. (c) Anslyn, E. V. *J. Org. Chem.* **2007**, *72*, 687–699.

(6) For recent examples of ratiometric pH sensor, see: (a) Charier, S.; Ruel, O.; Baudin, J.-B.; Alcor, D.; Allemand, J.-F.; Meglio, A.; Jullien, L. *Angew. Chem., Int. Ed.* **2004**, *43*, 4785–4788. (b) Charier, S.; Ruel, O.; Baudin, J.-B.; Alcor, D.; Allemand, J.-F.; Meglio, A.; Jullien, L.; Valeur, B. *Chem.—Eur. J.* **2006**, *12*, 1097–1113. (c) Evangelio, E.; Hernando, J.; Imaz, I.; Bardaji, G. G.; Alibés, R.; Busqué, F.; Ruiz-Molina, D. *Chem.—Eur. J.* **2008**, *14*, 9754–9763. (d) Bergen, A.; Granzhan, A.; Ihmels, H. *Photochem. Photobiol. Sci.* **2008**, *7*, 405–407.

(7) (a) Kavernos, G. J.; Turro, N. J. *Chem. Rev.* **1986**, *86*, 401. (b) Closs, G. L.; Miller, J. R. *Science* **1988**, *240*, 440–447. (c) Kavernos, G. J. *Photoinduced Electron Transfer*; VCH Publishers, New York, 1993. (d) Wasielewski, M. R. *J. Org. Chem.* **2006**, *71*, 5051–5066.

(8) (a) Kollmansberger, M.; Gareis, T.; Heinl, S.; Breu, J.; Daub, J. *Angew. Chem., Int. Ed.* **1997**, *36*, 1333–1334. (b) Baruah, M.; Qin, W.; Basarić, N.; De Borggraeve, W. M.; Boens, N. *J. Org. Chem.* **2005**, *70*, 4152–4157.

(9) (a) Czarnik, A. W. *Acc. Chem. Res.* **1994**, *27*, 302–310. (b) Guo, X.; Qian, X.; Jia, L. *J. Am. Chem. Soc.* **2004**, *126*, 2272–2273.

(10) Martinez-Manez, R.; Sancenon, F. *Chem. Rev.* **2003**, *103*, 4419–4476.

(11) (a) Ergen, E.; Weber, M.; Jacob, J.; Herrmann, A.; Müllen, K. *Chem.—Eur. J.* **2006**, *12*, 3707–3713. (b) Kuruvilla, E.; Nandajan, P. C.; Schuster, G. B.; Ramaiah, D. *Org. Lett.* **2008**, *10*, 4295–4298.

(12) Tusa, J. K.; He, H. *J. Mater. Chem.* **2005**, *15*, 2640–2647.

(13) Van den Berg, O.; Jager, W. F.; Picken, S. J. *J. Org. Chem.* **2006**, *71*, 2666–2676.

(14) (a) Jager, W. F.; van den Berg, O.; Picken, S. J. *Macromol. Symp.* **2005**, *230*, 11–19. (b) van den Berg, O.; Jager, W. F.; Cangialosi, D.; van Turnhout, J.; Verheijen, P. J. T.; Wübbenhorst, M.; Picken, S. J. *Macromolecules* **2006**, *39*, 224–231.

(15) (a) Carrigan, S.; Doucette, S.; Jones, C.; Marzzacco, C. J.; Halpern, A. M. *J. Photochem. Photobiol., A* **1996**, *99*, 29–35. (b) Jayaraman, S.; Verkman, A. S. *Biophys. Chem.* **2000**, *85*, 49–57.

(16) Palacios, M.; Wang, Z.; Montes, V. A.; Zyranov, G. V.; Anzenbacher, P. *J. Am. Chem. Soc.* **2008**, *130*, 10307–10314.

of this fluorescent chelator with various metal ions. Recently the use of substituted 6- and 7-aminoquinolines for the detection of Zn^{2+} and Cd^{2+} cations has been reported.[17]

On the basis of these findings it was recognized that the 7AMQ chromophore is an excellent choice for the construction of fluorescent sensors. The high fluorescence quantum yields Φ_F, up to 0.85, will ensure a strong emission signal, whereas the long fluorescence lifetimes τ_F, up to 13 ns, will enable the detection of relatively slow quenching processes. Also this cationic molecule is expected to have a high excited state reduction potential $E^*(S_1)_{red}$, which makes photoinduced electron transfer thermodynamically more favorable and generally increases the rate constant k_{ET}. An additional advantage is the flexible and versatile synthesis, which enables independent attachment of multiple functional groups to the chromophore at positions N7 and N1. In contrast to most chromophores, the 7-amino-1-methylquinolinium unit is inherently water-soluble, and all derivatives synthesized so far are water-soluble.

In this paper we report on the synthesis, photophysical properties, and sensor characteristics of the fluorescent pH sensors **3**, the first sensors based on the 7AMQ chromophore. A basic characterization of the 7AMQ chromophore has been obtained from spectral and photophysical data of **3** and model compounds **2** and **4**. In addition density functional theory (DFT) and semiempirical INDO/s calculations have been performed to describe the (photo)physical properties of **2**−**4** in the ground state and the locally excited state. Structure−property relationships, with respect to the magnitude of the dissociation constants in the ground state pK_A and in the excited state pK_A^*, and with respect to the magnitude of the fluorescence enhancement (FE) upon protonation, have been investigated. The photophysical properties of **3** will be compared with those of pH sensors based on other CT-chromophores.[18−21]

Results and Discussion

Design and Synthesis. In the pH sensors **3**, an oligomethylene spacer connects the chromophore to the amino receptor unit to which the substituents R^1 and R^2 are attached. The proton affinity of the amine, expressed by the dissociation constants pK_A and pK_A^*,[22] is determined by the electron affinity of R_1, R_2, and the spacer−chromophore moiety. By variation of R^1, R^2, and n, the dissociation constant pK_A^* can be tuned in a rational manner. The rate of electron transfer k_{ET} in the off-state, which will determine the fluorescence enhancement (FE), will decrease as the spacer length increases,[23] and an exponential decay of k_{ET} with distance is anticipated.[7d] The substituents R^1 and R^2 strongly influence k_{ET}. Faster electron transfer is generally observed for electron-rich amines that have low oxidation potentials.[7,24] Steric hindrance generally does not play a role, for PET processes, apart from those cases in which the gain in free energy is very small.[25] Therefore, the rates of electron transfer, and thereby the fluorescence enhancement of **3**, can be tuned in a rational manner by variation of R^1, R^2, and n. Along with the pH sensors **3**, the model compounds **2** and **4** were synthesized. Compounds **2** are used for investigating the photophysics of the 7AMQ chromophore. Compounds **4** are methylated on the same amines that are protonated at low pH values and thus mimick the behavior of the protonated pH sensors $\mathbf{3H}^+$ under a large variety of experimental conditions, including a high pH.

Compounds **2** and **3** were synthesized by a nucleophilic aromatic substitution in which the fluoride in **1** is displaced by a nitrogen from an aliphatic (di)amine, as depicted in Scheme 1. All compounds were isolated in high yield and purity by crystallization from the reaction mixture. In most cases monofunctional amines were used, i.e., compounds containing a single reactive amine, but for the synthesis of **3a**−**c**, difunctional amines were used. Formation of bichromophoric compounds was prevented by using a large excess of the respective diamines.[26] Compounds **4** were synthesized by reacting **3d**−**g** with methyliodide. The identity of all compounds was confirmed by NMR spectroscopy and by mass spectrometry, see the Supporting Information. In the mass spectra, only one parent paek of the cations of **2** and **3** is visible, whereas **4** shows up as 3 strong peaks. These are from the dication and the monocations after CH_3^+ and H^+ cleavage, respectively, see Table S1 (Supporting Information).

Photophysical Characterization. The absorption and emission spectra of **3a** at different pH values in water are shown in Figure 1. Upon protonation of the primary amine, the absorption spectra shift 13 nm to the blue, from 414 to 401 nm, and the emission spectra exhibit a 27 nm blue shift from 517 to 490 nm. These spectral shifts are caused by a decreased electron density on the amino receptor, which is efficiently transduced to N7. In the absorption spectra displayed in Figure 1 isosbestic points are clearly visible, which indicates the coexistence of only two species, **3a** and $\mathbf{3aH}^+$.

Along with the blue shifts, the emission is strongly enhanced upon protonation. For **3a** a 17-fold increase in fluorescence quantum yield Φ_F, from 0.05 to 0.85, is observed. This fluorescence enhancement is caused by photoinduced electron transfer (PET) from the receptor nitrogen to the chromophore in **3a**. In the protonated form $\mathbf{3aH}^+$, this process is inhibited.

(17) (a) Xue, L.; Jiang, H. *Org. Lett.* **2009**, *11*, 1655–1658. (b) Xue, L.; Liu, Q.; Jiang, H. *Org. Lett.* **2009**, *11*, 3454–3457.

(18) (a) de Silva, A. P.; Gunaratne, H. Q. N.; Habib-Jiwan, J.-L.; McCoy, C. P.; Rice, T. E.; Soumillion, J.-P. *Angew. Chem., Int. Ed.* **1995**, *34*, 1728–1731. (b) Daffy, L. M.; de Silva, A. P.; Gunaratne, H. Q. M.; Huber, C.; Lynch, P. L. M.; Werner, T.; Wolfbeis, O. S. *Chem.—Eur. J.* **1998**, *4*, 1810–1815. (c) de Silva, A. P.; Rice, T. E. *Chem. Commun.* **1999**, 163–164. (d) Niu, C.-G.; Zeng, G.-M.; Chen, L.-X.; Shen, G.-L.; Yu, R.-Q. *Analyst* **2004**, *129*, 20–24.

(19) O'Connor, N. A.; Sakata, S. T.; Zhu, H.; Shea, K. J. *Org. Lett.* **2006**, *8*, 1581–1584.

(20) (a) Callan, J. F.; de Silva, A. P.; Ferguson, J.; Huxley, A. J. M.; O'Brien, A. M. *Tetrahedron* **2004**, *60*, 11125–11131. (b) Uchiyama, S.; Iwai, K.; de Silva, A. P. *Angew. Chem. Int. Ed* **2008**, *47*, 4667–4669.

(21) (a) Qian, X.; Xiao, Y. *Tetrahedron Lett.* **2002**, *43*, 2991–2994. (b) Xiao, Y.; Qian, X. *Tetrahedron Lett.* **2003**, *44*, 2087–2091.

(22) In fluorescence measurements the dissociation constant in the excited state, pK_A^*, is determined. This is true under the assumption that excited state proton transfer (ESPT) is faster than fluorescence, which is generally the case, see: Kaneko S.; Yotoriyama, S.; Koda, H.; Tobita, S. *J. Phys. Chem. A* **2009**, *113*, 3021−3028.

(23) Onada, M.; Uchiyama, S.; Santa, T.; Imai, K. *Luminescence* **2002**, *17*, 11–14.

(24) Rehm, D.; Weller, A. *Ber. Bunsenges. Phys. Chem.* **1969**, *73*, 834–839.

(25) Pischel, U.; Zhang, X.; Hellrung, B.; Hasselbach, E.; Muller, P.-A.; Nau, W. M. *J. Am. Chem. Soc.* **2000**, *122*, 2027–2034.

(26) Bichromophoric compounds are synthesized efficiently, when **1** reacts with 0.5 equiv of 1,2-ethylenediamine, 1,3-propylenediamine, or 1,4-butylenediamine. Isolated yields were 75%, 83%, and 85%, respectively.

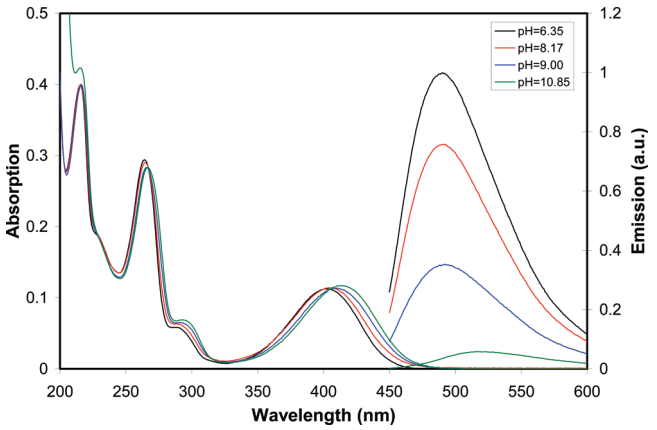

FIGURE 1. Absorption and emission spectra of **3a** in water at different pH values.

For compounds **3b**−**g**, a qualitatively similar behavior was observed, and results are shown in Tables 1 and 2. Shifts in emission and absorption wavelengths strongly decrease with the spacer length, and for **3c**, a compound that contains a butyl spacer, the spectral shifts in emission and absorption are reduced to a mere 3 nm. Also, the fluorescence enhancement upon protonation is strongly decreased upon increasing the spacer length. Spectral shifts upon protonation indicate that none of the pH sensors **3** are pure PET sensors. It should be noted that the spectroscopic properties of **4**, as displayed in Tables 1 and 2, are identical with those of the corresponding **3H**$^+$ compounds.

The fluorescence intensities of **3a**−**g** in water as a function of the pH are compiled in Figure 2. Emission and absorption spectra were recorded from pH 2 to 12, and the reverse titrations, from pH 12 to 2, were performed subsequently. Identical results, with respect to the dissociation constant and fluorescence enhancement, were obtained for both titrations (Figure S1, Supporting Information).[27] The pH-dependent emission intensities are described very accurately by eq 1, and the obtained dissociation constants pK_A* and fluorescence enhancements FA ($=I(HA^+)/I(A)$), are compiled in Table 1. At high pH values, above pH 10, the emission intensities for compounds like **3a**−**c**, **3e**, and **3g** are significantly lower than those calculated with eq 1, due to an additional quenching process. In Figure 2, the pH-dependent emission intensity of compound **4a**, which exhibits the same quenching process, is included to visualize the magnitude of this quenching.

For **3** dissociation constants range from 5.8 for **3f** to 9.9 for **3c** and these values are strongly determined by the electron affinity of the substituents R^1 and R^2 and the length of the spacers. Within each set of compounds, the primary amines are the strongest bases, followed by the dimethylamino and the morpholino compounds. This is completely in line with the reported dissociation constants for the model compounds methylamine (10.62),[28] trimethylamine (9.76),[28,29] and 4-methylmorpholine (7.40).[29] Obviously, the dissociation constants of **3a**, **3d**, and **3f** are significantly lower, due to the strongly electron deficient chromophore, which is connected with the base by a short ethylene spacer, an effect that has also been observed for similar fluorescent sensors based on other CT chromophores.[18−21]

TABLE 1. Chemical Yields and Spectroscopic Data of Compounds 2−4

		λ_{max}						
compd	yield	abs A[a]	em A[a]	abs AH^+	em AH^+	pK_A	pK_A*	FE[b] $I(HA^+)/I(A)$
2b	72	413	504					
2d	82	435	538					
3a	84	414	517	401	490	8.8	8.7	17
3b	83	415	503	409	497	9.6	9.5	4.9
3c	58	416	504	413	501	9.9	9.9	2.0
3d	84	409	507	401	487	8.3	8.1	54
3e	84	415	504	409	496	9.2	9.1	9.6
3f	87	412	504	400	487	5.9	5.8	56
3g	83	414	502	409	495	6.8	6.7	4.4
4a	64	402	486					
4b	78	407	496					
4c	46	400	487					
4d	64	407	495					

[a]A and AH^+ refer to the compound with an amine and an ammonium receptor, respectively. [b]The fluorescence enhancement FE, defined as $I(HA^+)/I(A)$, is determined upon excitation at 410 nm. The intensities $I(HA^+)$ and $I(A)$ are taken at the emission maximum λ_{max} for each species.

$$I_F = \frac{10^{(pK_A^* - pH)}}{1 + 10^{(pK_A^* - pH)}} I_F(HA^+) + I_F(A) \quad (1)$$

$$\lambda_{Abs} = \lambda_{Abs}(HA^+) \frac{10^{(pK_A - pH)}}{1 + 10^{(pK_A - pH)}} (\lambda_{Abs}(HA^+) - \lambda_{Abs}(A)) \quad (2)$$

The effect of the substituents R^1 and R^2 on the fluorescence enhancement is very pronounced and correlates with the oxidation potentials E_{ox} of the different receptors. According to the Rehm−Weller equation[24] (eq 3), a lower oxidation potential of the electron donor makes electron transfer more exorgenic, and this generally results in faster electron transfer. Primary amines have high oxidation potentials and are generally not employed as receptor units in pH sensor. Secondary amines are stronger electron donors, and tertiary amines are the strongest electron-donating amines.[30] Oxidation potentials within the group of tertiary amines decrease in the order alkyldimethylamine ≥ 4-alkylylmorpholine > alkyldiethylamine, and the fluorescence enhancement of fluorescent sensors bearing these groups increases accordingly. The high fluorescence enhancements observed for **3d** and **3f**, which contain a dimethylamino and a morpholino receptor, respectively, compared to that of the primary amino compound **3a**, are as expected. For compounds **3e**, **3g**, and **3b**, which contain the same receptor units attached with a C3 spacer, the same trend is observed, but fluorescent enhancements are lower. It should be noted that the fluorescence enhancements of **3** are significantly higher in comparison with fluorescent pH sensors based on CT chromophores. In fact, ethylamine-functionalized

(27) In all cases the emission intensity has decreased to ~95% of the original value after the forward and backward titration. This decrease in emission is most likely due to dilution.

(28) Hall, H. K. *J. Am. Chem. Soc.* **1957**, *79*, 5441–5444.

(29) Xu, F.; Otto, F. D.; Mather, A. E. *Can. J. Chem.* **1993**, *71*, 1048–1050.

(30) Beeson, J.; Huston, M. E.; Pollard, D. A.; Venkatachalam, T. K.; Czarnik, A. W. *J. Fluoresc.* **1993**, *3*, 65–68.

(31) Pfeffer, F. M.; Buschgens, A. M.; Barnett, N. W.; Gunnlaugsson, T.; Kruger, P. E. *Tetrahedron Lett.* **2005**, *46*, 6579–6584.

TABLE 2. Photophysical Properties of 2−4

	Φ_F[a] A	τ_F[b] A	k_F[a,c] A	k_{nr}[a,c] A	Φ_F[a] AH^+	τ_F[b] AH^+	k_F[a,c] AH^+	k_{nr}[a,c] AH^+
2b	0.59	11.5	5.1	3.6				
2d	0.04	0.8	5.0	120				
3a	0.05	0.2/5.0[e]	−[e]	−[e]	0.85	12.8	6.3	1.5
3b	0.16	2.8[d]	5.7	30	0.78	12.6	6.2	1.7
3c	0.31	6.0[d]	5.2	11.5	0.63	12.4	5.1	3.0
3d	0.016	0.14/5.0[e]	−[e]	−[e]	0.86	13.0	6.6	1.1
3e	0.08	1.35[d]	5.9	70	0.77	12.7	6.1	1.8
3f	0.015	0.25	6	395	0.84	12.9	6.5	1.2
3g	0.17	2.7	6.3	31	0.74	12.7	5.4	2.5
4a	0.82	13.0	6.3	1.4				
4b	0.76	12.8	6.0	1.9				
4c	0.81	13.0	6.2	1.5				
4d	0.77	12.7	6.1	1.8				

[a]Quantum yields, and the deactivation rates derived thereof, ±5%. [b]Lifetimes in ns. [c]Rate constants in 10^7 s^{-1}. [d]Estimated values corrected for OH^- quenching. [e]A single lifetime was not obtained.

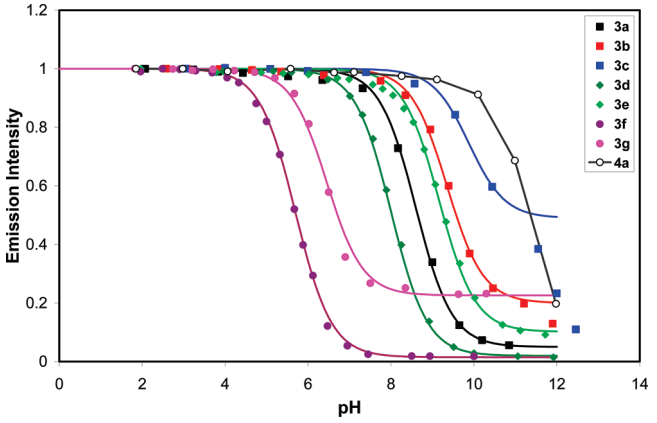

FIGURE 2. Emission intensities of **3** and **4a** as a function of the pH in water. The curves that connect the data points were obtained with eq 1.

compounds based on the 4-aminonaphthyl-1,8-imide (ANI),[31] 1-amino-4-nitrobenzoxadiazole (NBD),[32] and 1,5-aminonaphthalene sulfonamide (Dansyl)[19] chromophores have been prepared, but these compounds have not been employed as fluorescent pH sensors.[33] In this respect the high fluorescence enhancement of **3a** is remarkable. For fluorescent sensors with *N*,*N*-dimethylaminoethyl spacer−receptor units based on NBD,[20] 4-amino-1,8-dicyanonapthalene (ADCN),[21] ANI,[18] and Dansyl[19] chromophores, fluorescence enhancements of 40, 35, 14, and 12, respectively, have been reported. These values are markedly lower than the 55 reported for **3d** and the same observation has been made when comparing **3e**−**g** with fluorescent pH sensors that have morpholino receptors attached to CT chromophores.

$$\Delta G_{PET} = E_{ox} - E^*(S_1)_{red} + C \qquad (3a)$$

$$E^*(S_1)_{red} = E_{red} + E^*(S_1) \qquad (3b)$$

From absorption spectra the dissociation constants in the ground state, pK_A, were determined, using eq 2.[34] The absorption maxima for **3a**−**c** along with the calculated fits are shown in Figure 3. Table 1 shows that dissociation constants in the ground state pK_A were typically ∼0.1 pH unit higher than those in the excited state pK_A* for all compounds. This implies that these compounds are more basic in the ground state, and this observation is in line with the expected charge transfer in the excited state: from the quinolinium nitrogen N1 toward the aniline nitrogen N7, *vide infra*.

In addition to steady state fluorescence, fluorescence lifetime measurements were performed. The fluorescence decay was most accurately described by the biexponential function described by eq 3. However, for most compounds a slow decay was responsible for over 90% of the emission, see Table S2 (Supporting Information). Therefore we will describe the fluorescence decay by a monoexponential decay, unless specified otherwise. For all protonated amines **3aH**$^+$−**3gH**$^+$ as well as methylated compounds **4a**−**d**, lifetimes between 12.4 and 13.0 ns were measured. For the nonprotonated compounds **3**, lifetime determinations were complicated by a dynamic quenching process that takes place above pH 10. Only for **3f** and **3g**, which have dissociation constants pK_A* below 7, were lifetimes measured directly. For all other compounds, lifetimes were estimated after correcting for the extent of quenching.[35] For **3a** and **3d** we have not been able to determine a single lifetime at high pH values. For these compounds fast decay traces with 0.2 and 0.135 ns lifetimes were recorded, but they were accompanied by slower and rather persistent decay processes with a longer ∼5 ns lifetime.

Table 2 shows that upon protonation τ_F and Φ_F are proportional for most compounds. According to eqs 5a and 5b, this implies that the rate of fluorescence k_F has not been influenced by protonation of the receptor unit. For all compounds (**3**, **3H**$^+$, and **4**), k_F is 5−6.5 × 10^7 s^{-1}. Nonradiative decay rates k_{nr} for the protonated compounds **3H**$^+$ and the model compounds **4** are low, between 1 × 10^7 and 3 × 10^7 s^{-1}, which is indicative of weak inherent quenching. For the nonprotonated compounds **3** nonradiative decay rates between 1 × 10^8 and 4 × 10^9 s^{-1} are observed, depending on the spacer length. Nonradiative decay is due

(32) Cotté, A.; Bader, B.; Kuhlmann, J.; Waldmann, H. *Chem. Eur. J.* **1999**, *5*, 922–936.

(33) For 9-aminomethylanthracene a fluorescence enhancement of 0.4 has been reported. This compound has a C1 spacer and the estimated excited state reduction potential for the anthracene chromophore is −1.36 eV, see Ref 30.

(34) Please note that eq 2 is valid under the assumption that the absorption maximum λ_{abs} shifts linearly with the composition.

(35) The lifetime of the fast decay, originating from the nonprotonated base, was corrected for OH^- quenching. The deviation of the data points from the curves drawn by using eq 1, see Figure 2, was used to estimate the extent of OH^- quenching.

(36) See ref 2a, Chapter 8.

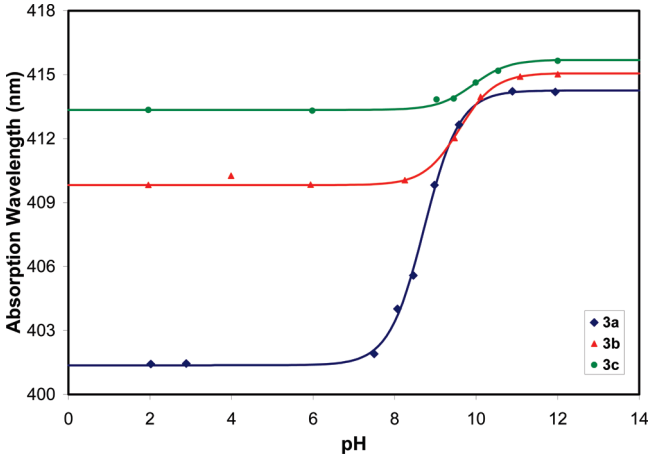

FIGURE 3. Absorption wavelengths λ_{max} of **3a**−**c** as a function of the pH in water. The curves that connect the data points were obtained with eq 2.

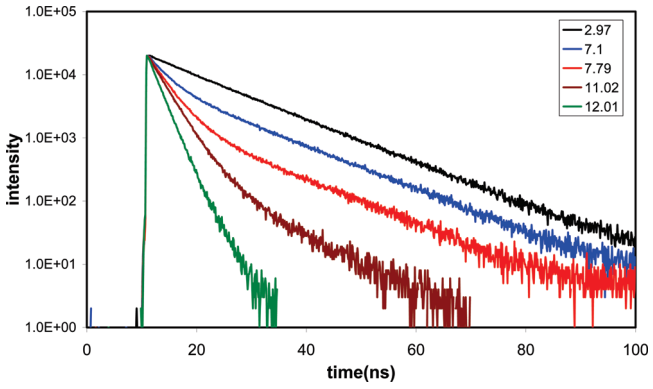

FIGURE 4. Time-dependent emission of **3g** in water as a function of pH.

to the electron transfer along with the inherent quenching processes. If we assume that the rate of the inherent quenching processes, just like the rate of fluorescence, has not been influenced by (de)protonation the quenching of **3** is dominated by intramolecular photoinduced electron transfer (PET) in all cases.

For compound **3g** the fluorescence decay was determined as a function of the pH. Since both **3g** and **3gH**$^+$ decay monoexponentially the presence of two emitting species at pH values around pK_A* is clearly visible in Figure 4. The dynamic quenching at pH values above 10 is also clearly visible, as the emission decays monoexponentially with a gradually decreasing lifetime. Obviously these lifetime measurements can be used for an accurate pH determination in two distict pH regions: around pK_A* (6.7) and above pH 10, see Figure S2 (Supporting Information).

A series of pH sensors based on the 4-aminonaphthyl-1,8-imide (ANI)[18] chromophore, which bear ethyl spacers and diethylamino, dimethylamino, and morpholino receptor units, respectively, have been characterized in H_2O−MeOH (1:1). For these compounds, comparable with **3d** and **3f**, fluorescence quantum yields Φ_F of 0.7, rates of fluorescence k_F of 1×10^8 s^{-1}, and rates of electron transfer k_{ET} of $\sim 1.5 \times 10^9$ s^{-1} were reported. The lower fluorescence enhancements of the ANI-based sensors, around 12, are explained by the

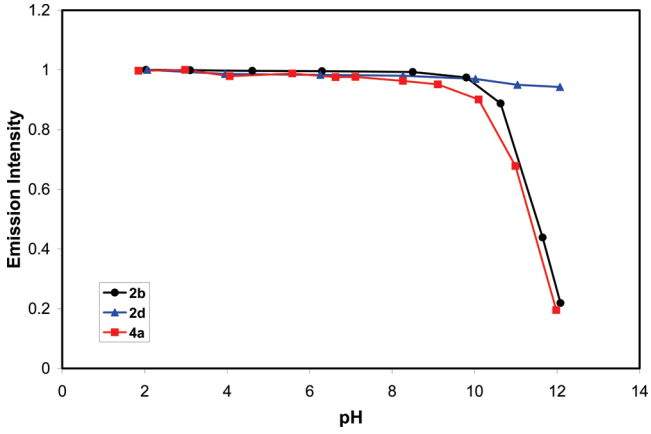

FIGURE 5. Emission intensities of **2b**, **2d**, and **4a** as a function of pH.

lower quantum yields, the higher rates of fluorescence, and the lower rates of electron transfer combined. This reduced electron transfer rate may be a consequence of the lower excited state reduction potential $E^*(S_1)_{red}$ of the ANI chromophore, see Table S4 (Supporting Information).

$$I_F = b_1 e^{-t/\tau_1} + b_2 e^{-t/\tau_2} \quad (4)$$

$$\Phi_F = \frac{k_F}{k_F + k_{nr}}; \quad \tau_F = \frac{1}{k_F + k_{nr}};$$

$$k_F = \frac{\Phi_F}{\tau_F}; \quad k_{nr} = \frac{1 - \Phi_F}{\tau_F} \quad (5a\text{−}d)$$

Fluorescence Quenching by OH$^-$ Ions. In addition to the expected *intra*molecular quenching by PET from the deprotonated[20] receptor, an additional quenching process at high pH values has been observed for **3**, model compounds **4**, and the nonfunctionalized compounds **2a**−**c**, but not for **2d**, see Figure 5. The OH$^-$ quenching was characterized by the following observations. No changes in the absorption spectra were observed, indicating that changes in the ground state do not take place. Emission spectra did not shift in wavelength, but decreased in intensity only, which is indicative of quenching of the locally excited state. From the Stern−Volmer plots depicted in Figure 6, very high quenching constants k_q were obtained with use of eq 6. From Table S3 (Supporting Information), which compiles the results extracted from Figure 6, it is clear that higher quenching constants are found for more electron deficient systems. Finally, time-resolved emission experiments revealed that the fluorescence lifetime decreases steadily upon increasing the pH, which proves that the quenching process is dynamic.[36]

$$\frac{I_0}{I} - 1 = K_{SV}[OH^-]K_{SV} = k_q \tau_0 \quad (6)$$

Fluorescence quenching by OH$^-$ ions may be due to intermolecular PET,[37] or caused by deprotonation in the excited state, provided that a nonemitting conjugated base is formed. If the first process takes place the quenching rates should scale with the oxidation potential of the quencher, and the expected sequence for a series of anions should be $k_q[I^-] > k_q[Br^-] > k_q[OH^-] > k_q[Cl^-]$. If, on the other hand, deprotonation takes place, the basicity

(37) Shizuka, H.; Obuchi, H. *J. Phys. Chem.* **1982**, *86*, 1297–1302.

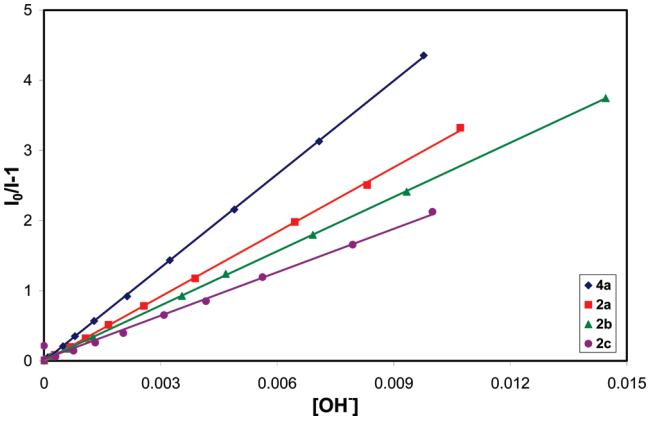

FIGURE 6. Stern−Volmer plots for compounds **2a**−**c** and **4a**, as a function of [OH^-] in NaOH solutions in water.

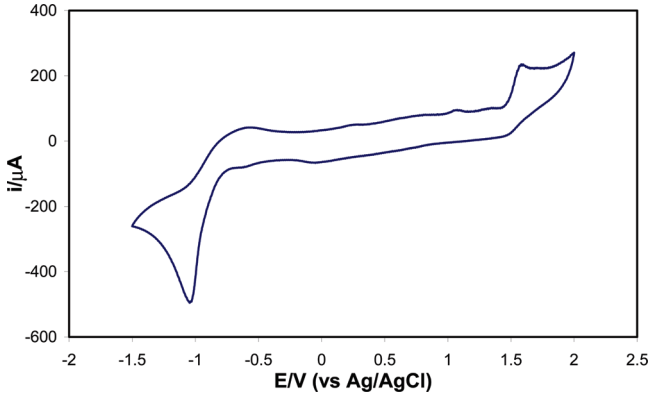

FIGURE 7. Cyclic voltamogram of **2b** in acetonitrile-TBA-BF_4 solution.

of the quenching anion[38] is relevant and one would expect $k_q[OH^-] \gg k_q[Cl^-] > k_q[Br^-] > k_q[I^-]$. For both mechanisms the rate of quenching will also increase as the quinolinium ion gets more electron deficient, because that will increase the acidity of the N7 proton.

In Figure S3 (Supporting Information), the quenching of **2b** by the different anions is represented in a Stern−Volmer plot. The order of quenching rates is $k_q[OH^-] > k_q[I] \gg k_q[Br^-] > k_q[Cl^-]$, and it is clear that quenching by these different anions takes place by deprotonation *and* PET, However, the observation that the hydroxide quenching is 2−3 orders of magnitude faster than the bromide quenching proves that hydroxide quenching is due to excited state deprotonation of **2b** exclusively. It is concluded that the decrease in fluorescence of **3**, **4**, and **2a**,**b** at high pH values is due to excited state deprotonation at N7, which forms a nonfluorecent species. This deprotonation can be explained by the cationic, highly electron deficient nature of the chromophore, in combination with charge transfer from N1 to N7. Both phenomena strongly decrease the electron density at N7 and increase the acidity of the N7 proton in the excited state. It should be noted that due to this process compounds **3** are effectively dibasic pH sensors.

Reduction Potentials[39] of the 7AQ Chromophore. The reduction potential of **2b** was determined with cyclic voltametry[40] in acetonitrile, see Figure 7. For this compound a wave at −1.1 V versus Ag/AgCl was recorded that was assigned to the 7AMQ reduction. At high voltage, above 1.5 V, an oxidation process is visible that is assigned to the oxidation of the 7-amino group. A reduction potential of the *N*-methylquinolinium ion in water was reported at −0.86 V,[15b] and for various 3- and 6-substituted derivatives, values between −0.45 and −1.06 V were reported.[15a] These values reveal that *N*-methylquinolinium ions have high reduction potentials. The relatively low value found for **2b** is obviously due to the electron-donating nature of the 7-amine that is in conjugation with the pyridinium acceptor.

An excited state reduction potential $E^*(S_1)_{red}$ of 1.60 eV for **2b** was obtained by using eq 3b. According the well-known Rehm−Weller equation (eq 3a),[24] this value implies that PET processes with electron donors that have oxidation potentials below ∼1.55 eV are thermodynamically allowed for **2b**. Lower excited state reduction potentials $E^*(S_1)_{red}$ of −1.43, −1.1, and −1.55 eV were reported for the ANI,[41] the Dansyl,[42] and the NBD[43] chromophore, respectively (Table S4, Supporting Information). The implications are that weaker electron donors, like primary amines, are able to quench the fluorescence of **2b**, and that for 7AMQ-based sensors higher electron transfer rates k_{ET} are expected with identical electron donors.

Calculations

Density functional theory (DFT) and semiempirical INDO/s calculations were undertaken, in order to obtain additional insight in the photophysics of the 7AMQ chromophore. The ground state geometry of compound **2d** was fully optimized by DFT calculations and it was found that the dimethylamino group assumes a planar conformation, with both methyl carbons in the same plane as the quinolinium moiety, see Figure S4 (Supporting Information). The lone pair on the nitrogen in the dimethyl amino contributes to the π-system, and therefore is an integral part of the chromophore.

The lowest three optical absorption bands for **2d** were calculated by INDO/s-CIS calculations. The results are listed in Table 3. The lowest excited state (state 2) occurs at 407 nm and is strongly allowed, with an oscillator strength of 0.48. This lowest excited state almost exclusively consists of the excitation of a single electron from HOMO to the LUMO, as indicated by the main CI-coefficients. The second excited state is forbidden by symmetry, while the third is allowed but at a much shorter wavelength (282 nm). These values are in fair agreement with the strong absorptions observed at 435 and 273 nm, and a minor absorption at 303 nm.[44]

(38) Anslyn, E. V.; Doughety, D. A. *Modern Physical Organic Chemistry*; University Science Books: Sausalito, CA, 2006; Chapter 5.

(39) Reduction potentials E_{red} are versus the Ag/AgCl reference electrode, excited state reduction potentials $E^*(S_1)_{red}$ are versus the standard hydrogen electrode (SHE).

(40) Compton, R. C.; Banks, C. E. *Understanding Voltammetry*; World Scientific: Hackensack, NJ, 2007.

(41) Saha, S.; Samanta, A. *J. Phys. Chem. A* **2002**, *106*, 4763–4771.

(42) Ceroni, P.; Laghi, I.; Maestri, M.; Balzani, V.; Gestermann, S.; Gorka, M.; Vögtle, F. *New J. Chem.* **2002**, *26*, 66–75.

(43) Ramachandram, B.; Samanta, A. *J. Phys. Chem. A* **1998**, *102*, 10579.

(44) It should be noted that calculated absorption maxima are in vacuum, whereas experiments were performed in water.

(45) (a) Pina, F.; Bernardo, M. A.; Garćia-España, E. *Eur. J. Inorg. Chem.* **2000**, 2143–2157. (b) Pina, F.; Lima, J. C.; Lodeiro, C.; de Melo, J. S.; Díaz, P.; Albelda, M. T.; Garćia-España, E. *J. Phys. Chem. A* **2002**, *106*, 8207–8212.

(46) Yuan, D.; Brown, R. G. *J. Phys. Chem. A* **1997**, *101*, 3461–3466.

TABLE 3. Excitation Energies, Oscillator Strengths, and Main CI Expansion Coefficients for the Excitation of 2d

transition	ΔE (eV)	λ (nm)	f	main CI coefficient
1 → 2	3.04	407	0.48	0.95 (H → L)
1 → 3	3.81	325	0.00	0.70 (H-2 → L) + 0.56 (H → L+1)
1 → 4	4.39	282	0.63	0.62 (H-2 → L) − 0.72 (H → L+1)

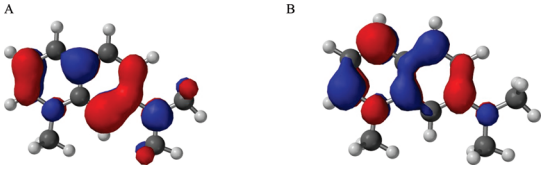

FIGURE 8. HOMO and LUMO orbitals calculated for **2d** (A and B).

The HOMO and LUMO obtained from the INDO calculations are shown in Figure 8. For **2d** the HOMO has considerable amplitude on the dimethylamino group whereas the LUMO is mostly localized on the quinolinium part of the molecule. This means, that upon excitation of an electron from the HOMO to the LUMO, some positive charge shifts from the quinolinium part of the molecules to the dimethylamino part; however, a fully charge separated state is not formed. This is also reflected in the Mulliken charge distributions in the ground and first excited states obtained from the INDO calculation depicted in Figure 9. Although the charge on the nitrogen in the dimethylamino becomes more positive there is no complete shift of the positive charge to N7. This limited charge transfer is confirmed experimentally by the small differences in the dissociation constants in the excited state (pK_A^*) and in the ground state (pK_A).

The optical absorption spectra of **3d** and **3dH**$^+$ were calculated in order to determine the effect of protonation on the absorption spectrum. For both **3d** and **3dH**$^+$ excitation from the ground state to the first excited state is strongly allowed, and in both cases this excited state corresponds to the excitation of an electron from the highest occupied molecular orbital (HOMO) to the lowest unoccupied molecular orbital (LUMO). Protonation leads to an increase in the excitation energy for the lowest state from 3.11 eV (398 nm, $f = 0.44$) for **3d** to 3.41 eV (364 nm, $f = 0.39$) for **3dH**$^+$. These calculated values are in reasonable agreement with the experimental values of 409 and 401 nm, respectively. This red shift can be rationalized by examining the HOMO orbitals for **3d** and **3dH**$^+$, which are shown in Figure 10. For **3d** the HOMO has considerable amplitude on both the nitrogen atoms attached to the ethylene spacer, indicating that both nitrogens are electronically coupled. Protonation removes this coupling completely and the HOMO is less delocalized.

Discussion

The fluorescent sensors **3** are highly sensitive water-soluble pH sensors with dissociation constants between 5.8 and 9.9. These dissociation constants are tuned in a straightforward manner by changing the electronic nature of the substituents R^1 and R^2 and the length of the spacer. Extending the range of dissociation constants to higher pH values will not be of practical value due to the quenching at pH ~11, caused by excited state deprotonation at N7. Obtaining lower dissociation constants can be accomplished by attaching polyamine receptors at N7.[45]

Fluorescence enhancements between 2 and 55 have been reported for **3**, and these values are significantly higher than those for pH sensors based on other CT chromophores,

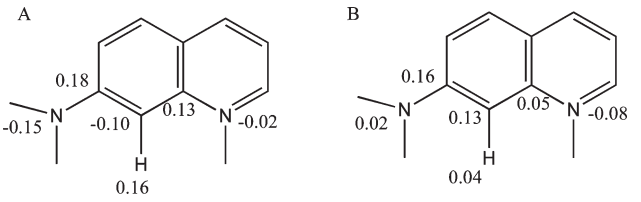

FIGURE 9. Mulliken charges in ground state (A) and first excited state (B) in **2d**.

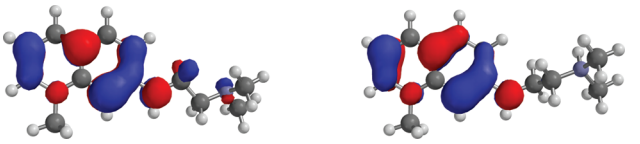

FIGURE 10. HOMO orbitals calculated for **3d** (a) and **3dH**$^+$ (b).

which bear identical spacer−receptor units. The fully protonated compounds **3H**$^+$ are highly fluorescent with fluorescence quantum yields Φ_F between 0.75 and 0.85. These high quantum yields are due to the absence of inherent quenching, quantified by low rates of nonradiative decay k_{nr} of 1×10^7 to 3×10^7 s^{-1}. For the nonprotonated compounds **3** low fluorescence quantum yields Φ_F (as low as 0.015) have been reported. These low quantum yields are caused by two factors: relatively high rates of electron transfer k_{ET}, up to 4×10^9 s^{-1}, and relatively low rates of fluorescence k_F, around 6×10^7 s^{-1}, see eq 5a. The low rate of fluorescence is an inherent property of the 7AMQ chromophore, whereas the high rates of electron transfer k_{ET} may be explained by the high excited state reduction potential $E^*(S_1)_{red}$ (1.6 eV) of the 7AMQ chromophore, which makes electron transfer to the excited chromophore highly exorgenic and increases the rate of PET quenching.

Finally, it should be noted that fluorescent pH sensors based on other CT chromophores were usually characterized in mixtures of water with organic solvents, typically MeOH−H_2O. The solvent may have a strong effect on the photophysics of CT chromophores. For example, an increased solvent polarity[46] generally results in enhanced rates of nonradiative decay, lower quantum yields, and lower fluorescence enhancements. It is therefore appropriate to conclude that the 7-AMQ chromophore *and* water as the solvent determine the photophysical properties of **3**.

Conclusions

We have synthesized a series of water-soluble fluorescent pH sensors **3**, based on the 7-amino-1-methylquinolinium (7AMQ) chromophore, in high yield and purity by a nucleophilic aromatic substitution of aliphatic diamines on 7-fluoro-1-methylquinolinium iodide **1**. Compounds **3** have high fluorescence quantum yields in the protonated state, between 0.75 and 0.85, and high fluorescence enhancements upon protonation, up to 55. The benign properties of **3**, notably the high fluorescence enhancement, in comparison with similar sensors based on CT chromophores, have been explained from the photophysics of the 7AMQ chromophore, notably the absence of inherent quenching, the low rates of fluorescence, and the high excited state reduction potential.

A remarkable feature of the 7AMQ-based pH sensors is the excited state deprotonation of an amine proton at N7.[47]

This process has been explained by the cationic, highly electron deficient nature of the chromophore, in combination with charge transfer from N1 to N7. Due to this process compounds **3** are effectively dibasic pH sensors. A very practical advantage of the 7AMQ chromophore is that all pH sensors based on this chromophore are water-soluble.

We finally conclude that 7AMQ is an excellent chromophore for the construction of highly sensitive inherently water-soluble PET sensors. Since this CT chromophore is asymmetric, the sensitivity 7AMQ-based sensors is expected to be strongly dependent on the position at which the spacer−receptor will be attached.[18,19] Future work will explore the attachment of functional groups at N1 and N7 and the subsequent construction of smart sensors and molecular logic devices.

Experimental Section

UV−Vis and IR Spectroscopy. UV−visible characterization was performed with a double beam spectrophotometer. Samples were measured in deionized water with use of a quartz cell (1 cm optical path). IR spectra were taken in KBr pellets with an FT-IR spectrophotometer.

Fluorescence Spectroscopy. Fluorescence spectra were recorded with a fluorescence spectrometer equipped with a standard 90° setup at room temperature. For the quantum yield determinations a fixed excitation wavelength of 400 nm and fixed slit widths (1 nm excitation, 1 nm emission) were chosen, and dye solutions were prepared with an absorptions below 0.1. The relative quantum yields were calculated from the integrated emission intensity (I_{em}) and the transmission (T) of the specific sample at 400 nm, using the following equation:

$$\Phi_{rel.} = \frac{I_{em}*(1-T_{ref.})*n}{I_{ref.}(1-T)*n_{ref.}} \quad (7)$$

As a reference 9,10-diphenylanthracene (DPA) in cyclohexane (quantum yield 0.86)[48] was used. For pH-dependent fluorescence measurements solutions with an optical density of 0.1 at 400 nm in 200 mL of 10^{-4} M KH_2PO_4 buffer were prepared. The solution was acidified with HCl down to a pH of ∼2, basified with KOH solution up to pH ∼12, then subsequently acidified back to pH ∼2. The pH was monitored with a pH meter. At regular intervals both the emission and absorption were measured by taking ca. 3 mL of solution in a quarz cuvette. For all emission spectra the excitation wavelength λ_{ex} was 410 nm. For all compounds dissociation constants (pK_A* values) were determined with use of eq 1.

Lifetime measurements were performed by using samples identical with those used for pH-dependent fluorescence measurements. Fluorescence decay curves were obtained after excitation with a 405 nm pulsed solid-state laser and lifetimes were obtained by fitting these curves with eq 4. Rates of fluorescence k_F and rates of fluorescence quenching k_Q, were obtained with use of eq 5a−d.

Computational Details. The geometry of all fluorescent sensors was fully optimized by density functional theory (DFT) calculations, using the BLYP exchange correlation functional with Dunning's cc-pVDZ basis set.[49] All geometry optimizations were performed with the Gaussian98 program package. The excitation energies for the fluorescent sensors were calculated by singly excited configuration interaction (CIS) calculations, using a reference wave function from intermediate neglect of differential overlap (INDO) calculations.[50] In the INDO-CIS calculations the geometries from the DFT were used.

Cyclic Voltametry. Cyclic voltametric measurements were carried out in acetonitrile with the help of a computer-driven potentiostat. The scan rate was kept at 0.05 V s^{-1}. The working electrode and the auxiliary electrode were platinum electrodes. All redox potentials were measured with respect to the Ag/AgCl electrode. Tetrabutylammonium tetrafluoroborate (10^{-1} M) was used as the support electrolyte. The concentration of the measured compound was $\sim 10^{-3}$ M. Solutions were deoxygenated before the measurements by purging Argon.

Synthesis and Characterization. TLC analysis was performed on silica gel, and ^{1}H and ^{13}C NMR spectra were measured in DMSO or D_2O at 300/400 and 75/100 MHz. Chemical shifts are given in ppm (δ) relative to tetramethylsilane (TMS) as internal standard (DMSO) or calibrated on *t*-BuOH as the internal standard (D_2O). LC-MS data were collected with a Liquid Chromatrograph Mass Spectrometer, with a diode-array detector. The column used was the Xbridge Shield RP 18.5 mm (4.6 × 150 mm) on 95/5 MeOH−H_2O. Fast Atom Bombardment (FAB) mass spectrometry was carried out with a four-sector mass specrometer, coupled to a system program. Samples were loaded in a matrix solution (3-nitrobenzyl alcohol) onto a stainless steel probe and bombarded with Xenon atoms with an energy of 3KeV.

During the high-resolution FAB-MS measurements a resolving power of 10 000 (10% valley definition) was used.

The synthesis of **1**, **2a**, **2d**, and **3a** is published elsewhere.[13] Unless mentioned otherwise all quinolinium salts were synthesized in 96% ethanol with 250 or 500 mg of **1**, 1.05−1.1 equiv of amine, and 1.1 equiv of triethylamine. The products were obtained by crystallization from 96% ethanol unless mentioned otherwise. The methylations of **3d−g** were performed by dissolving **3** in a minimum amount of dry ethanol or methanol and adding an excess of methyl iodide. The product **4** crystallizes out of solution and is isolated by filtration.

7-(Butylmino)-1-methylquinolinium Iodide (2c). 7-Fluoro-1-methylquinolinium iodide (**1**, 250 mg, 0.86 mmol), butylamine (150 mg, 1.03 mmol), and triethylamine (95 mg, 94 mmol) in 96% ethanol (5 mL) were heated to reflux for 30 min. The reaction mixture was allowed to cool to room temperature. After addition of 2 mL of diethyl ether, orange crystals were formed and 255 mg (86%) of **2c** was obtained after filtration. Mp 188−191 °C. ^{1}H NMR (400 MHz, DMSO-d_6) δ (ppm) 8.89 (1H, dd, J_1 = 6.3 Hz, J_2 = 0.9 Hz), 8.68 (1H, d, J = 7.8 Hz), 7.98 (1H, d, J = 9.3 Hz), 7.90 (1H, t, J = 5.1 Hz), 7.45 (1H, dd, J_1 = 7.8 Hz, J_2 = 6.0 Hz), 7.37 (1H, dd, J_1 = 9.0 Hz. J_2 = 1.5 Hz), 6.70 (1H, s), 4.29 (3H, s), 3.30 overlap with H_2O (2H, m), 1.65 (2H, q, J = 7.3 Hz), 1.43 (J = 7.4 Hz), 0.95 (3H, t, J = 7.3 Hz). ^{13}C NMR (100 MHz DMSO-d_6) δ (ppm) 155.3, 147.1, 144.3, 143.0, 131.9, 123.7, 122.2, 115.5, 91.4, 44.8, 43.0, 30.6, 20.5, 14.43. HRMS m/z calcd for $C_{14}H_{19}N_2^+$ 215.1548, found 215.1550. Anal. Calcd for $C_{14}H_{19}IN_2$ (342.22): C, 49.14; H, 5.60; N, 8.19. Found: C, 49.28; H, 5.61; N, 8.20.

7-(2-Morpholinoethylamino)-1-methylquinolinium Iodide (3f). 7-Fluoro-1-methylquinolinium iodide (**1**, 500 mg, 1.73 mmol), 2-morpholinoethylamine (247 mg, 1.90 mmol), and triethylamine (192 mg, 94 mmol) in 96% ethanol (5 mL) were heated to reflux for 30 min. The reaction mixture was allowed to cool to room temperature, and 580 mg (87%) of **3f** was obtained after

(47) A similar deprotonation of N1 in NBD systems that results in additional quenching at high pH values has been reported. In this case, however, deprotonation occurs in the ground state, see ref 20.

(48) Morris, J. V.; Mahaney, M. A.; Huber, J. R. *J. Phys. Chem.* **1976**, *80*, 969.

(49) Dunning, T. H. *J. Chem. Phys.* **1989**, *90*, 1007.

(50) (a) Bacon, A. D.; Zerner, M. C. *Theor. Chim. Acta.* **1979**, *53*, 21. (b) Zerner, M. C. In *Reviews in Computational Chemistry*; Boyd, L., Ed.; VCH: New York, 1991; p 313. (c) Edwards, W. D.; Zerner, M. C. *Theor. Chim. Acta.* **1987**, *72*, 347.

filtration. Mp 206−208 °C. ^{1}H NMR (300 MHz, DMSO-d_6) δ (ppm) 8.92 (1H, d, J = 6.3 Hz), 8.71 (1H, d, J = 7.8 Hz), 8.01 (1H, d, J = 9.3 Hz), 7.82 (1H, t, J = 5.1 Hz), 7.48 (1H, dd, J_1 = 7.8 Hz, J_2 = 6.0 Hz), 7.41 (1H, dd, J_1 = 9.3 Hz, J_1 = 1.8 Hz), 6.79 (1H, broad) 4.31 (3H, s), 3.62 (4H, t, J = 4.5 Hz), 3.47 (2H, dd, J = 6.1 Hz), 2.64 (2H, t, J = 6.4 Hz), 2.49 (4H, t, J = 4.4 Hz). ^{13}C NMR (100 MHz, DMSO-d_6) δ (ppm) 155.0, 146.9, 144.2, 142.8, 131.6, 123.5, 122.3, 115.4, 91.5, 66.6, 56.7, 53.8, 44.9. HRMS m/z calcd for $C_{16}H_{22}N_3O^+$ 272.1783, found 272.1768. Anal. Calcd for $C_{16}H_{22}IN_3O$ (399.27): C, 48.13; H, 5.55; N, 10.52. Found: C, 48.03; H, 5.60; N, 10.55.

4-Methyl-4-(3-(1-methylquinolinium-7-ylamino)propyl)morpholin-4-ium Iodide (4d). Compound **3g** (100 mg, 0.24 mmol) was dissolved in 5 mL of methanol, and methyl iodide (0.2 mL, 3.2 mmol) was added. After 2 days at room temperature 86 mg (64%) of **4d** was isolated by filtration. Mp 243−244 °C. ^{1}H NMR (DMSO-d_6) δ (ppm) 8.96 (1H, d, J = 6.0 Hz), 8.75 (1H, d, J = 7.6 Hz), 8.06 (1H, d, J = 9.2 Hz), 7.98 (1H, t, J = 4.8 Hz), 7.52 (1H, dd, $J_1 \approx J_2$ = 7.0 Hz), 7.39 (1H, d, J = 9.2 Hz), 6.81 (1H, broad), 4.36 (3H, s), 3.96 (4H, b), 3.69 (2H, dd, J = 8.2 Hz), 3.49 (6H, br), 3.20 (3H, s), 2.11 (2H, m, J = 8.0 Hz). ^{13}C NMR (100 MHz, DMSO-d_6) δ (ppm) 154.6, 147.1, 144.4, 142.7, 131.8, 123.6, 122.0, 115.7, 113.7, 92.0, 61.9, 60.3, 59.7, 53.8, 47.1, 45.0, 20.7. HRMS calcd for $C_{18}H_{27}I_2N_3O^+$ 428.1199, found 428.1196.

Acknowledgment. We thank Ruben Abellon for assisting with the time-resolved fluorescence experiments, Louw Florisse for technical assistance, and Corrado Locati for performing the CV measurements on **2b**.

Supporting Information Available: Synthetic procedures, NMR spectra, LC-MS data, HR-MS and fluorescence lifetimes for all compounds and titration curves, IR spectra, and fluorescence decay traces of **2c**, **3b**, **3f** and **4c**. This material is available free of charge via the Internet at http://pubs.acs.org.